Mechatronics 30 (2015) 286–296

Contents lists available at ScienceDirect

Mechatronics

journal homepage: www.elsevier.com/locate/mechatronics

Gain-scheduled robust control for lateral stability of four-wheel-independent-drive electric vehicles via linear parameter-varying technique

Xian Jian Jin [a], Guodong Yin [a,b,*], Nan Chen [a]

[a] School of Mechanical Engineering, Southeast University, Nanjing 211189, China
[b] State Key Laboratory of Automotive Safety and Energy, Tsinghua University, Beijing 100084, China

ARTICLE INFO

Article history:
Received 20 May 2014
Revised 24 December 2014
Accepted 29 December 2014
Available online 24 January 2015

Keywords:
Electric vehicles
Lateral stability
Robust control
Gain-scheduled
Linear parameter-varying technique

ABSTRACT

This paper proposes a robust gain-scheduled H_∞ controller for lateral stability control of four-wheel-independent-drive electric vehicles via linear parameter-varying technique. The controller aims at tracking the desired yaw rate and vehicle sideslip angle by controlling the external yaw moment. In the design of controller, uncertain factors such as vehicle mass and tire cornering stiffness in vehicle lateral dynamics are represented via the norm-bounded uncertainty. To address the importance of time-varying longitudinal velocity for vehicle lateral stability control, a linear parameter-varying polytopic vehicle model is built, and the built vehicle model depends affinely on the time-varying longitudinal speed that is described by a polytope with finite vertices. In order to reduce conservative, the hyper-rectangular polytope is replaced by a hyper-trapezoidal polytope. Simultaneously, the quadratic *D*-stability is also applied to improve the transient response of the closed-loop system. The resulting gain-scheduling state-feedback controller is finally designed, and solved utilizing a set of linear matrix inequalities derived from quadratic H_∞ performance and *D*-stability. Simulations using Matlab/Simulink-Carsim® are carried out to verify the effectiveness of the proposed controller with a high-fidelity, CarSim®, full-vehicle model. It is found from the results that the robust gain-scheduled H_∞ controller suggested in this paper provides improved vehicle lateral stability, safety and handling performance.

1. Introduction

Emerging four-wheel-independent-drive electric vehicles have appeared as promising vehicle architectures based on several advantages in terms of high energy efficiency and advanced vehicle dynamics control [1,2]. FWID-EVs (four-wheel-independent-drive electric vehicles) utilize in-wheel motors to drive the wheels such that the torque of each wheel can be controlled independently. Such a flexible actuation can be easily used to generate the external yaw moment with the torque differences between the left and right wheels, which possesses potential to improve lateral stability of FWID-EVs [1–4]. Lateral stability control of vehicle dynamics is a very important aspect of improving vehicle handling and safety performance. A great deal of research on vehicle lateral dynamics stability control, including direct yaw moment control system or active steering control with steer-by-wire system, has been done in recent years [2–10].

Although the above research achievements were successful, there are still two main challenges about the lateral dynamics stability control. The first one is inherent nonlinearities in the vehicle lateral dynamics model such as tire nonlinearity. Most research papers employ linear tire model that assumes tire cornering stiffness is a fixed value. In fact, when the vehicle undergoes high accelerations under extreme driving maneuvers, tire's dynamics nature presents inherent nonlinearity that means a changed tire cornering stiffness. If lateral tire force in this nonlinear region is treated as linear, the lateral stability may be lost, and the behaviors of the vehicle will become uncontrollable and very dangerous. The second one is that most published research on lateral stability control focused on the fixed longitudinal velocity, while time-varying longitudinal velocity is also very critical for the tracking performance in controlling lateral stability of vehicle dynamics, since longitudinal velocity has a pronounced effect for the vehicle handling and safety performance, especially for heavy steering in high speed [6,8]. In addition, according to [10,11], in contrast to conventional vehicles, the hulking transmission and mechanical link between source of power and actuator for FWID-EVs have been

* Corresponding author at: School of Mechanical Engineering, Southeast University, Nanjing 211189, China.

http://dx.doi.org/10.1016/j.mechatronics.2014.12.008
0957-4158/

removed and replaced with X-by-wire system, which leads to substantially reduced vehicle inertial parameters (e.g., vehicle mass and yaw moment of inertia), and the FWID-EVs become lightweight. Furthermore, it means that the effects of variation in inertial parameters for lateral stability and handling performance of FWID-EVs become much more pronounced. Thus, designing the lateral stability controller is demanded to consider uncertainties such as tire cornering stiffness, vehicle mass and yaw moment of inertia, and the controller is also needed to consider the tradeoff between the tracking performance and robustness against uncertainties.

Robust control theory has been proved to be a powerful technique in dealing with the above mentioned challenges, several linear and nonlinear robust controllers have been reported, such as H_∞ methodology, μ-synthesis approach, mixed H_∞/GH_2 control, sliding mode control, input output linearization and nonlinear adaptive robust control [12–18].

However, on the one hand, utilizing robust control of linear time invariant techniques has the major drawback that unusually assumes the fixed operating longitudinal velocity, which is difficult to cope with above descriptive the second challenge. On the other hand, nonlinear robust control possesses capability of handling nonlinearities of lateral dynamics model and uncertainties in vehicle parameters. Whereas, the design of nonlinear robust controller is complex and challenged, and these nonlinear robust techniques fail to take advantage of the reality that the vehicles lateral dynamics are closer to linear under normal driving conditions [19,20].

Recently, the linear parameter-varying technique whose theoretical developments in the context of robust control has attracted the increasing concern from the academia. Main advantage of the LPV (linear parameter-varying) technique is in allowing application of powerful linear synthesis concepts to nonlinear systems, which can be successfully used to automatically schedule the gain of the controller with respect to variation of scheduling variable, have shown promising perspective in various applications [21–23]. As for LPV-based robust control on lateral stability control, few investigations have been reported. Utilizing LPV technique and linear tire model, gain-scheduled active differential and steering controller, slip-controller, global chassis controller are proposed, respectively [24–29].

This paper proposes a robust gain-scheduled H_∞ controller for lateral stability control of FWID-EVs by controlling the external yaw moment. Uncertainties in vehicle lateral dynamics, including tire cornering stiffness, vehicle mass and moment of inertia about the yaw axis, are considered simultaneously. To design robust gain-scheduled controller, and LPV-based polytopic vehicle model is built. The quadratic D-stability is also applied to improve the transient response of the closed-loop system simultaneously. Finally, gain-scheduling state-feedback H_∞ controller is designed, which is solved utilizing a set of linear matrix inequalities (LMIs).

The schematic diagram of overall control structure is shown in Fig. 1. The remainder of the paper is organized as follows. Section 2 presents LPV-based uncertain vehicle model. In Section 3, robust gain-scheduled H_∞ controller is design. In Section 4, simulation results are presented and discussed. Finally, conclusions are offered in Section 5 (see Table 1).

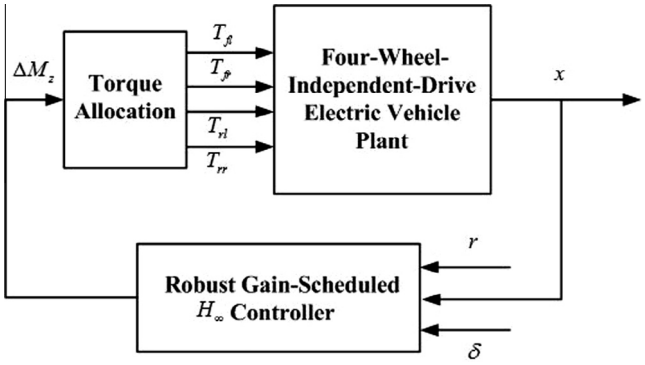

Fig. 1. Schematic diagram of overall control structure.

Table 1
The parameters for the experimental electric vehicles.

Parameter	Value
Vehicle total mass m	960 kg
Distance, the CG to front and rear axle, L_f, L_r	1.1 m, 1.3 m
Vehicle moment of inertia about yaw axis I_z	625.3 kg m^2
Front and rear tires cornering stiffness C_f, C_r	25,325 N/rad, 27,280 N/rad

2. Uncertain vehicle dynamics model

2.1. Vehicle dynamics model

In contrast to conventional vehicles, FWID-EVs with in-wheel motors shown in Fig. 2 possess flexile drive architecture that the torque of each wheel can be controlled independently, and the external yaw moment with the torque differences between the left and right wheels can be easily generated, which can be applied to control lateral stability. To simplify designing the controller, the widely used single track model shown in Fig. 2 is chosen in this study [4,12], the vehicle lateral dynamics equations that include lateral and yaw motions can be written as:

$$\begin{aligned} mV_x(\dot{\beta}+\gamma) &= F_{yf}+F_{yr} \\ I_z\dot{\gamma} &= l_fF_{yf}-l_rF_{yr}+\Delta M_z \end{aligned} \tag{1}$$

where m is vehicle total mass, V_x, γ and β are vehicle longitudinal velocity, yaw rate and vehicle side slip angle at center of gravity, respectively. F_{yf} and F_{yr} are the lateral tire force for front and rear wheels, respectively. I_z, L_f and L_r are vehicle moment of inertia about yaw axes, the distances from the CG (center of gravity) to the front and rear axle respectively. ΔM_z is the external yaw moment.

Under normal driving conditions, accelerations of the vehicle are low, the tire slip angles tend to small, and the tire operates in this linear region. At small slip angles, the tire slip angles can be expressed as the following:

$$\begin{aligned} \alpha_f &= \delta-\frac{l_f\gamma}{V_x}-\beta \\ \alpha_r &= \frac{l_r\gamma}{V_x}-\beta \end{aligned} \tag{2}$$

where α_f and α_r are the tire slip angle for front and rear tires, respectively.

When the tire operates in linear region, the lateral tire forces can be linearly approximated as follows:

$$\begin{aligned} F_{yf} &= C_f\alpha_f \\ F_{yr} &= C_r\alpha_r \end{aligned} \tag{3}$$

where C_f and C_r are the tire cornering stiffness for front and rear tires, respectively.

Substituting (2) and (3) into (1), the state-space representation of vehicle lateral dynamics system can be written as follows:

$$\dot{x}(t) = Ax(t)+B_1\omega(t)+B_2u(t) \tag{4}$$

where

$$x(t) = [\beta,\gamma]^T$$

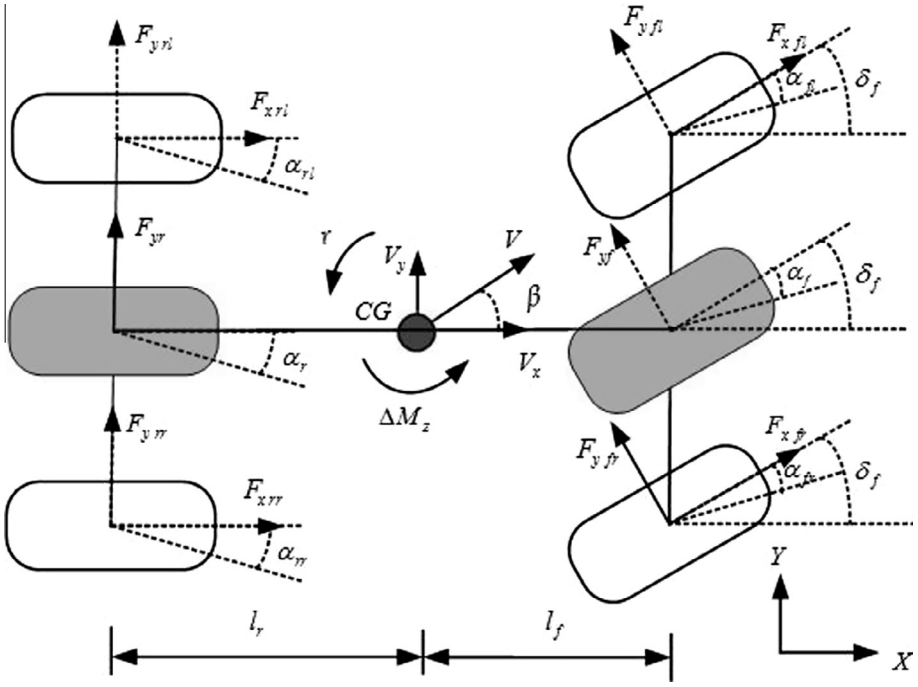

Fig. 2. The yaw model of vehicle lateral dynamics.

$$\omega(t) = \delta, \quad u(t) = \Delta M_z$$

$$A = \begin{bmatrix} -\frac{C_f + C_r}{mV_x} & \frac{l_r C_r - l_f C_f}{mV_x^2} - 1 \\ \frac{l_r C_r - l_f C_f}{I_z} & -\frac{l_f^2 C_f + l_r^2 C_r}{I_z} \end{bmatrix}$$

$$B_1 = \begin{bmatrix} \frac{C_f}{mV_x} \\ \frac{l_f C_f}{I_z} \end{bmatrix}, \quad B_2 = \begin{bmatrix} 0 \\ \frac{1}{I_z} \end{bmatrix}$$

2.2. LPV-based uncertain vehicle dynamics model

Fig. 3 describes the lateral tire force versus the tire slip angle, the importance of tire nonlinearity in the tire model can be observed. At small tire slip angle, the lateral tire force of the linear model has the nearly same level as that of the nonlinear model. It is appropriate for small tire slip angles to use a fixed tire cornering stiffness. Based on this fact, most research papers employ the linear tire model. However, when vehicle undergoes high accelerations, the tire slip angle continues to grow, and the tire cornering stiffness begins to change, simultaneously, the lateral tire force of the linear model has a distinct difference than that of the nonlinear model, and then the lateral tire force becomes nonlinear. If tire model makes use of a fixed tire cornering stiffness in this nonlinear region, that is, lateral tire force in this nonlinear region is treated as linear, the lateral stability may be lost, and the uncontrollable vehicle will become very dangerous.

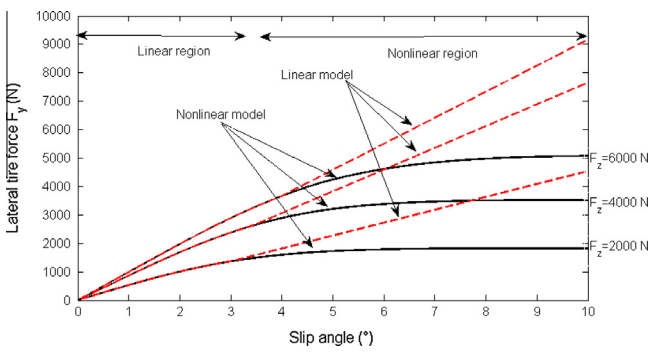

Fig. 3. The lateral tire force versus the tire slip angle.

To deal with the problem of tire nonlinearity, nonlinear models include Dugoff and Pacejka tire models have been developed and applied, nevertheless, the two nonlinear tire models requires a large number of tire-specific parameters that are usually unknown [7,20]. Moreover, the design of nonlinear robust controller will become more complex and challenged. In this study, tire nonlinearity can be handled using the uncertain tire cornering stiffness, which are represented via the norm-bounded uncertainty as follows:

$$\begin{aligned} C_f &= C_{fe} + N(t)\widetilde{C}_{fn} \\ C_r &= C_{re} + N(t)\widetilde{C}_{rn} \end{aligned} \tag{5}$$

where

$$C_{fe} = \frac{C_{fmax} + C_{fmin}}{2}, \quad C_{re} = \frac{C_{rmax} + C_{rmin}}{2}$$

$$\widetilde{C}_{fn} = \frac{C_{fmax} - C_{fmin}}{2}, \quad \widetilde{C}_{rn} = \frac{C_{rmax} - C_{rmin}}{2}$$

C_{fmax} and C_{rmax} are the maximal tire cornering stiffness for front and rear tires, and C_{fmin} and C_{rmin} are minimal cornering stiffness for front and rear tires, respectively. $N(t)$ satisfy $|N(t)| \leqslant 1$.

Similarly, using the maximum mass m_{max} and the minimum mass m_{min}, the uncertain vehicle mass can be represented by

$$\frac{1}{m} = m_e + N(t)\tilde{m}_n \tag{6}$$

where

$$m_e = \frac{1}{2}(m_{smax} + m_{smin}), \quad m_{smax} = \frac{1}{m_{min}}$$

$$\tilde{m}_n = \frac{1}{2}(m_{smax} - m_{smin}), \quad m_{smin} = \frac{1}{m_{max}}$$

According to [29], the moment of inertia is proportional to the mass, thus the uncertain moment of inertia can be written as:

$$\frac{1}{I_z} = i^2 m_e + N(t) i^2 \tilde{m}_n \tag{7}$$

where i^2 is relevant coefficient between that the mass and the moment of inertia.

For the state-space representation in Eq. (4), considering the uncertain term C_f/m as:

$$\begin{aligned}\frac{C_f}{m} &= (C_{fe} + N(t)\tilde{C}_{fn})(m_e + N(t)\tilde{m}_n) \\ &= C_{fe} m_e + (C_{fe}\tilde{m}_n + \tilde{C}_{fn} m_e) N(t) + \tilde{C}_{fn}\tilde{m}_n N^2(t)\end{aligned} \tag{8}$$

Note that the variations $\tilde{C}_{fn}$ and $\tilde{m}_n$ are small. Thus, the multiplying of $\tilde{C}_{fn}$ and $\tilde{m}_n$ is relatively much smaller than $C_{fe}\tilde{m}_n$ and $\tilde{C}_{fn} m_e$, and then the Eq. (8) is approximated as:

$$\frac{C_f}{m} \approx c_f m_0 + \Delta c_{fm} N(t) \tag{9}$$

where

$$c_f = C_{fe},\ m_0 = m_e,\ \Delta c_{fm} = C_{fe}\tilde{m}_n + \tilde{C}_{fn} m_e + \tilde{C}_{fn}\tilde{m}_n$$

Similarly, the uncertain term C_r/m can be approximated as:

$$\frac{C_r}{m} \approx c_r m_0 + \Delta c_{rm} N(t) \tag{10}$$

where

$$c_r = C_{re}, m_0 = m_e,\ \Delta c_{rm} = C_{re}\tilde{m}_n + \tilde{C}_{rn} m_e + \tilde{C}_{rn}\tilde{m}_n$$

As mentioned in Section 1, most published research on lateral stability control focused on the fixed longitudinal velocity, but time-varying longitudinal velocity is also very critical for the vehicle handling and safety performance. Since time-varying longitudinal velocity can be measured utilizing real-time sensors [9,10]. In this study, a robust gain-scheduled controller is designed to schedule the online measured longitudinal speed V_x.

Assuming that the variable range of longitudinal velocity V_x is $[\underline{V}_x,\ \overline{V}_x]$, and then the variable ranges of $1/V_x$ and $1/V_x^2$ are $[1/\overline{V}_x,\ 1/\underline{V}_x]$ and $[1/\overline{V}_x^2,\ 1/\underline{V}_x^2]$, respectively. Fig. 4 describes the hyper-rectangular polytope of the parameter set $(1/V_x,\ 1/V_x^2)$, i.e., MQPN. Using the linear combination of the four vertices, all the possible variable value in the domain can be represented. Note that

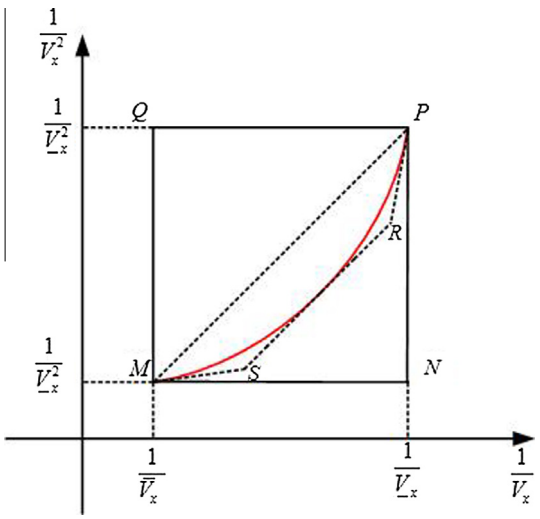

Fig. 4. Structure of the polytope.

the possible variable value of the set $(1/V_x,\ 1/V_x^2)$ only choice along the trajectory (the red line), it is clear that most area of the hyper-rectangular cannot be achieved, thus, the parameter set $(1/V_x,\ 1/V_x^2)$ depicted by hyper-rectangular polytope is conservative. To reduce conservative, the area that includes the trajectory of the parameter set $(1/V_x,\ 1/V_x^2)$ should be chosen as small as possible, here the hyper-rectangular polytope is replaced by a hyper-trapezoidal polytope. The new hyper-trapezoidal polytope is limited by the domain MPRS, the first edge MP is determined by the two points $M(1/\overline{V}_x,\ 1/\overline{V}_x^2)$ and $P(1/\underline{V}_x,\ 1/\underline{V}_x^2)$, and other two edges MS and PR are the tangents at points M and P, respectively. The last edge RS is the line that is parallel to the line MP and the tangent at the hyperbole.

By solving above line equations on the four edges, the coordinates of two new vertices R and S can be obtained:

$$\begin{aligned}R &= \left(\frac{1}{V_{x,R}}, \frac{1}{V_{x,R}^2}\right) \\ &= \left(\frac{\overline{V}_x^2 + 2\underline{V}_x\overline{V}_x - 3\underline{V}_x^2}{4(\underline{V}_x^2\overline{V}_x + \underline{V}\,\underline{V}_x^2 - 2\overline{V}_x)}, \frac{\underline{V}_x + \overline{V}_x}{4\underline{V}_x\overline{V}_x}\left(\frac{\overline{V}_x^2 + 2\underline{V}_x\overline{V}_x - 3\underline{V}_x^2}{\underline{V}_x^2\overline{V}_x + \underline{V}_x\underline{V}_x^2 - 2\overline{V}_x} + \frac{\underline{V}_x + \overline{V}_x}{\underline{V}_x\overline{V}_x}\right)\right)\end{aligned}$$

$$\begin{aligned}S &= \left(\frac{1}{V_{x,S}}, \frac{1}{V_{x,S}^2}\right) \\ &= \left(\frac{\underline{V}_x^2 + 2\underline{V}_x\overline{V}_x - 3\overline{V}_x^2}{4(\underline{V}_x^2\overline{V} + \underline{V}\,\underline{V}_x^2 - 2\underline{V}_x)}, \frac{\underline{V}_x + \overline{V}_x}{4\underline{V}_x\overline{V}_x}\left(\frac{\underline{V}_x^2 + 2\underline{V}_x\overline{V}_x - 3\overline{V}_x^2}{\underline{V}_x^2\overline{V} + \underline{V}\,\underline{V}_x^2 - 2\underline{V}_x} + \frac{\underline{V}_x + \overline{V}_x}{\underline{V}_x\overline{V}_x}\right)\right)\end{aligned}$$

Based on the four edges, the new hyper-trapezoidal polytope MPRS is built. Utilizing the new vertices $M(1/\overline{V}_x,\ 1/\overline{V}_x^2)$, $P(1/\underline{V}_x,\ 1/\underline{V}_x^2)$, $R(1/V_{x,R},\ 1/V_{x,R}^2)$ and $S(1/V_{x,S},\ 1/V_{x,S}^2)$, all the possible variable value of the parameter set $(1/V_x,\ 1/V_x^2)$ can be represented.

To design the robust gain-scheduled controller, two scheduled time-varying parameters are chosen as: $\rho_1(t) = 1/V_x$, $\rho_2(t) = 1/V_x^2$, and $\rho = [\rho_1\ \rho_2]^T$. Considering uncertainties in vehicle dynamics model, the LPV-based state-space representation of vehicle lateral dynamics system can be written as follows:

$$\begin{aligned}\dot{x}(t) &= (A(\rho) + \Delta A(\rho))x(t) + (B_1(\rho) + \Delta B_1(\rho))\omega(t) + (B_2 + \Delta B_2)u(t) \\ &= \sum_{i=1}^{4}\alpha_i(\rho)((A_i + \Delta A_i)x(t) + (B_{1,i} + \Delta B_{1,i})\omega(t) + (B_{2,i} + \Delta B_{2,i})u(t))\end{aligned} \tag{11}$$

where

$$\begin{cases}\alpha_1(t) = [|\rho_1(t) - \underline{\rho}_1(t)||\rho_2(t) - \underline{\rho}_2(t)|]/\tilde{\rho} \\ \alpha_2(t) = [|\bar{\rho}_1(t) - \rho_1(t)||\rho_2(t) - \underline{\rho}_2(t)|]/\tilde{\rho} \\ \alpha_3(t) = [|\rho_1(t) - \underline{\rho}_1(t)||\bar{\rho}_2(t) - \rho_2(t)|]/\tilde{\rho} \\ \alpha_4(t) = [|\bar{\rho}_1(t) - \rho_1(t)||\bar{\rho}_2(t) - \rho_2(t)|]/\tilde{\rho} \\ \tilde{\rho} = (\bar{\rho}_1 - \underline{\rho}_1)(\bar{\rho}_2 - \underline{\rho}_1)\end{cases}$$

$$A_1 = \begin{bmatrix} -\frac{c_f m_0 + c_r m_0}{\underline{V}_x} & \frac{l_r c_r m_0 - l_f c_f m_0}{\underline{V}_x^2} - 1 \\ l_r i^2 c_r m_0 - l_f i^2 c_f m_0 & -\frac{l_f i^2 c_f m_0 + l_r i^2 c_r m_0}{\underline{V}_x} \end{bmatrix} \quad B_{1,1} = \begin{bmatrix} \frac{c_f m_0}{\underline{V}_x} \\ l_f i^2 c_f m_0 \end{bmatrix}$$

$$A_2 = \begin{bmatrix} -\frac{c_f m_0 + c_r m_0}{V_{x,R}} & \frac{l_r c_r m_0 - l_f c_f m_0}{V_{x,R}^2} - 1 \\ l_r i^2 c_r m_0 - l_f i^2 c_f m_0 & -\frac{l_f i^2 c_f m_0 + l_r i^2 c_r m_0}{V_{x,R}} \end{bmatrix}, \quad B_{1,2} = \begin{bmatrix} \frac{c_f m_0}{V_{x,R}} \\ l_f i^2 c_f m_0 \end{bmatrix}$$

$$A_3 = \begin{bmatrix} -\frac{c_f m_0 + c_r m_0}{V_{x,S}} & \frac{l_r c_r m_0 - l_f c_f m_0}{V_{x,S}^2} - 1 \\ l_r i^2 c_r m_0 - l_f i^2 c_f m_0 & -\frac{l_f i^2 c_f m_0 + l_r i^2 c_r m_0}{V_{x,S}} \end{bmatrix}, \quad B_{1,3} = \begin{bmatrix} \frac{c_f m_0}{V_{x,S}} \\ l_f i^2 c_f m_0 \end{bmatrix}$$

$$A_4=\begin{bmatrix} -\frac{c_f m_0+c_r m_0}{\overline{V}_x} & \frac{l_r c_r m_0-l_f c_f m_0}{\overline{V}_x^2}-1 \\ l_r i^2 c_r m_0-l_f i^2 c_f m_0 & -\frac{l_f i^2 c_f m_0+l_r i^2 c_r m_0}{\overline{V}_x} \end{bmatrix},\quad B_{1,4}=\begin{bmatrix} \frac{c_f m_0}{\overline{V}_x} \\ l_f i^2 c_f m_0 \end{bmatrix}$$

$$\Delta A_1=L_{1,1}\overline{N}(t)H_{1,1}$$

$$L_{1,1}=\begin{bmatrix} -\frac{\Delta c_{fm}+\Delta c_{rm}}{\overline{V}_x} & \frac{l_r\Delta c_{rm}-l_f\Delta c_{fm}}{\overline{V}_x^2} \\ l_r i^2\Delta c_{rm}-l_f i^2\Delta c_{fm} & -\frac{l_f i^2\Delta c_{fm}+l_r i^2\Delta c_{rm}}{\overline{V}_x} \end{bmatrix},\quad B_{2,1}=\begin{bmatrix} 0 \\ i^2 m_0 \end{bmatrix}$$

$$\overline{N}(t)=\begin{bmatrix} N(t) & 0 \\ 0 & N(t) \end{bmatrix},\quad H_{1,1}=H_{1,2}=H_{1,3}=H_{1,4}=I$$

$$\Delta B_{1,1}=L_{2,1}\overline{N}(t)H_{2,1},\quad L_{2,1}=\begin{bmatrix} \frac{\Delta c_{fm}}{\overline{V}_x} & 0 \\ 0 & l_f i^2\Delta c_{fm} \end{bmatrix},\quad H_{2,1}=\begin{bmatrix} 1 \\ 1 \end{bmatrix}$$

$$\Delta A_2=L_{1,2}\overline{N}(t)H_{1,2}$$

$$L_{1,2}=\begin{bmatrix} -\frac{\Delta c_{fm}+\Delta c_{rm}}{V_{x,R}} & \frac{l_r\Delta c_{rm}-l_f\Delta c_{fm}}{V_{x,R}^2} \\ l_r i^2\Delta c_{rm}-l_f i^2\Delta c_{fm} & -\frac{l_f i^2\Delta c_{fm}+l_r i^2\Delta c_{rm}}{V_{x,R}} \end{bmatrix}$$

$$\Delta B_{1,2}=L_{2,2}\overline{N}(t)H_{2,2},\quad L_{2,2}=\begin{bmatrix} \frac{\Delta c_{fm}}{V_{x,R}} & 0 \\ 0 & l_f i^2\Delta c_{fm} \end{bmatrix},\quad H_{2,2}=H_{2,1}$$

$$\Delta A_3=L_{1,3}\overline{N}(t)H_{1,3}$$

$$L_{1,3}=\begin{bmatrix} -\frac{\Delta c_{fm}+\Delta c_{rm}}{V_{x,S}} & \frac{l_r\Delta c_{rm}-l_f\Delta c_{fm}}{V_{x,S}^2} \\ l_r i^2\Delta c_{rm}-l_f i^2\Delta c_{fm} & -\frac{l_f i^2\Delta c_{fm}+l_r i^2\Delta c_{rm}}{V_{x,S}} \end{bmatrix}$$

$$\Delta B_{1,3}=L_{2,3}\overline{N}(t)H_{2,3},\quad L_{2,3}=\begin{bmatrix} \frac{\Delta c_{fm}}{V_{x,S}} & 0 \\ 0 & l_f i^2\Delta c_{fm} \end{bmatrix},\quad H_{2,3}=H_{2,1}$$

$$\Delta A_4=L_{1,4}\overline{N}(t)H_{1,4}$$

$$L_{1,4}=\begin{bmatrix} -\frac{\Delta c_{fm}+\Delta c_{rm}}{\overline{V}_x} & \frac{l_r\Delta c_{rm}-l_f\Delta c_{fm}}{\overline{V}_x^2} \\ l_r i^2\Delta c_{rm}-l_f i^2\Delta c_{fm} & -\frac{l_f i^2\Delta c_{fm}+l_r i^2\Delta c_{rm}}{\overline{V}_x} \end{bmatrix}$$

$$\Delta B_{1,4}=L_{2,4}\overline{N}(t)H_{2,4},\quad L_{2,4}=\begin{bmatrix} \frac{\Delta c_{fm}}{\overline{V}_x} & 0 \\ 0 & l_f i^2\Delta c_{fm} \end{bmatrix},\quad H_{2,4}=H_{2,1}$$

$$B_{2,1}=\begin{bmatrix} 0 \\ i^2 m_0 \end{bmatrix},B_{2,1}=B_{2,2}=B_{2,3}=B_{2,4},\ \Delta B_{2,1}=L_{3,1}\overline{N}(t)H_{3,1}$$

$$\Delta B_{2,1}=\Delta B_{2,2}=\Delta B_{2,3}=\Delta B_{2,4}$$

$$L_{3,1}=\begin{bmatrix} 0 & 0 \\ 0 & i^2\tilde{m}_n \end{bmatrix},\quad H_{3,1}=\begin{bmatrix} 1 \\ 1 \end{bmatrix}$$

3. Robust gain-scheduled H_∞ controller

To improve lateral stability control and handling performance of the vehicle, the main control objective is to track the desired yaw rate and vehicle sideslip angle. Note that various sideslip angle estimation approaches are available [30,31], For instance, based on onboard vision system in the literature [30], the multirate estimator of vehicle body slip angle is proposed for electric vehicles, and the effectiveness of the proposed estimator is demonstrated by both simulations and experiments. Defining desired references $r=[\gamma_d\ \beta_d]^T$, also defining the new augmented states $\chi=[\chi_1(t)\ \chi_2(t)]^T$, where

$$\chi_1(t)=r-x,\quad \chi_2(t)=\int_0^t(r-x)dt \tag{12}$$

Thus, the gain-scheduled state-feedback control law for LPV system can be written as

$$\begin{aligned} cu(t)&=K(\rho)\chi(t)\\ &=K_1(\rho)(r-x)+K_2(\rho)\int_0^t(r-x)dt \end{aligned} \tag{13}$$

where $K(\rho)$ is the gain that depend on the scheduled parameters ρ_1 and ρ_2 to be designed. It is necessary to mention that the dimension of control law can be matched, because the dimension of ΔM_z in equation (4) is 1×1, and in Eq. (13) the dimension of $K(\rho)$ is 1×2, and then the dimension of $\chi(t)$ is 2×1, thus the dimension of $u(t)$ is 1×1. As can be seen in (13), the control law is a generalized proportional-integral control that can eliminate the tracking error. Moreover, such a design can avoid the NP (Non-deterministic Polynomial)-hard problem.

Substituting (13) into (11) gives the state-space representation of the closed-loop system as

$$\begin{aligned} \dot{\chi}(t)&=A_{\chi c}(\rho)\chi(t)+B_{1\chi c}(\rho)\omega(t)\\ z(t)&=C\chi(t) \end{aligned} \tag{14}$$

where

$$A_{\chi c}(\rho)=A(\rho)+\Delta A(\rho)\ +B_{2c}K(\rho)$$

$$B_{1\chi c}(\rho)=B_1(\rho)+\Delta B_1(\rho)$$

$$A_\Xi(\rho)=A(\rho)+B_{2C}$$

$$B_{2c}=B_2+\Delta B_2,\quad C=[1\quad 1]^T$$

To realize the tradeoff between the tracking performance and robustness against uncertainties for the controller. The H_∞ performance of the robust gain-scheduled controller chosen as:

$$\|z\|_2\leqslant\eta\|\delta\|_2 \tag{15}$$

To deal with the external disturbance and uncertainties, the robust gain-scheduled feedback H_∞ controller is designed by using the above index η and the following lemmas.

Lemma 1 (*Quadratic $H\infty$ performance [19,32]*). For a given index η, the gain-scheduling state-feedback controller exists such that the closed-loop system in (14) is asymptotically stable and possesses H_∞ level η form w to z for all variable values of the parameter vector ρ, if and only if a symmetric positive definite matrix P can be found to satisfy the following conditions:

$$\begin{bmatrix} A_{\chi c}^T(\rho)P+PA_{\chi c}(\rho) & PB_{1\chi c}(\rho) & C^T \\ * & -\eta^2 I & 0 \\ * & * & I \end{bmatrix}<0 \tag{16}$$

Lemma 2 (*[19,20]*). Let $\Gamma=\Gamma^T$, $\bar{\Upsilon}$ and $\bar{\vartheta}$ are real matrices with compatible dimensions, and $\widehat{N}(t)$ satisfying $|\widehat{N}(t)|\leqslant 1$. Then the following condition:

$$\Gamma+\bar{\Upsilon}\widehat{N}(t)\bar{\vartheta}+\bar{\vartheta}^T\widehat{N}(t)\bar{\Upsilon}^T<0 \tag{17}$$

holds if and only if there exists a positive scalar $\varepsilon>0$ such that

$$\begin{bmatrix} \Gamma & \varepsilon\bar{\Upsilon} & \bar{\vartheta}^T \\ * & -\varepsilon I & 0 \\ * & * & -\varepsilon I \end{bmatrix} < 0 \tag{18}$$

In the design of tracking controller, the transient response of the closed-loop system can be significantly effect by the eigenvalues [30]. Meanwhile, considering the physical limitations on the actuators, and the control input is also needed to be restricted. Thus, *D*-stability of the closed-loop system is studied.

Definition 1 (*LMI Regions*). [33]: An LMI region that is a subset D of the complex plane can be defined as follows:

$$D = \{s \in C : f_D(s) < 0\} \tag{19}$$

where

$$f_D(s) := \psi_1 + s\psi_2 + \bar{s}\psi_2^T$$

For the real application, some typical LMI regions have the following form:

(1) Half-plane $Re(s) < -\vartheta : f_D(s) := 2\vartheta + s + \bar{s} < 0$
(2) Disk centered at $(-q,0)$ with radius r

$$f_D(s) := \begin{bmatrix} -r & q+s \\ q+\bar{s} & -r \end{bmatrix} < 0 \tag{20}$$

(3) Conic sector with an apex at the origin and inner angle of 2θ

$$f_D(s) := \begin{bmatrix} \sin\theta(s+\bar{s}) & \cos\theta(s-\bar{s}) \\ \cos\theta(\bar{s}-s) & \cos\theta(s+\bar{s}) \end{bmatrix} < 0 \tag{21}$$

Lemma 3 (*Quadratic D-stability [33]*). The matrix is *D*-stable if and only if there exists a symmetric matrix P such that

$$M(A_{\chi c}(\rho), P) = \psi_1 \otimes P + \psi_2 \otimes (PA_{\chi c}(\rho)) + \psi_2^T \otimes (A_{\chi c}^T(\rho)P) < 0 \tag{22}$$

Specifically, the condition for the *D*-stability of a disk LMI region (q,r) can be written as

$$\begin{bmatrix} -rX & qX + XA_{\chi c}(\rho) \\ qX + XA_{\chi c}^T(\rho) & -rX \end{bmatrix} < 0 \tag{23}$$

To further design the controller, denoting

$$\Xi = A_\Xi(\rho)R + RA_\Xi^T(\rho) \tag{24}$$

Theorem 1. For the closed-loop system in (14), the gain-scheduling state-feedback controller exists such that the closed-loop system is quadratic *D*-stability in the disk centered at $(-q,0)$ with a radius r and possesses quadratic H_∞ performance η form w to z for all variable values of the parameter vector ρ, if and only if $\varepsilon(\rho)$, R and a symmetric positive definite matrix Q can be found to satisfy the following conditions:

$$\begin{bmatrix} \Xi & B_1(\rho) & C^T & \varepsilon_1(\rho)L_1(\rho) & \varepsilon_2(\rho)L_3(\rho) & (H_1(\rho)R)^T & 0 & \varepsilon_3(\rho)L_2(\rho) & (H_2(\rho)R)^T \\ * & -\eta^2 I & 0 & 0 & 0 & 0 & (H_3(\rho))^T & 0 & 0 \\ * & * & I & 0 & 0 & 0 & 0 & 0 & 0 \\ * & * & * & -\varepsilon_1(\rho)I & 0 & 0 & 0 & 0 & 0 \\ * & * & * & * & -\varepsilon_2(\rho)I & 0 & 0 & 0 & 0 \\ * & * & * & * & * & -\varepsilon_1(\rho)I & 0 & 0 & 0 \\ * & * & * & * & * & * & -\varepsilon_2(\rho)I & 0 & 0 \\ * & * & * & * & * & * & * & -\varepsilon_3(\rho)I & 0 \\ * & * & * & * & * & * & * & * & -\varepsilon_3(\rho)I \end{bmatrix} < 0 \tag{25}$$

$$\begin{bmatrix} -rQ & qQ + A_\Xi(\rho)Q & \varepsilon_4(\rho)L_1(\rho) & 0 & \varepsilon_5(\rho)L_2(\rho) & 0 \\ * & -rQ & 0 & (H_1(\rho)Q)^T & 0 & (H_2(\rho)Q)^T \\ * & * & -\varepsilon_4(\rho)I & 0 & 0 & 0 \\ * & * & * & -\varepsilon_4(\rho)I & 0 & 0 \\ * & * & * & * & -\varepsilon_5(\rho)I & 0 \\ * & * & * & * & * & -\varepsilon_5(\rho)I \end{bmatrix} < 0 \tag{26}$$

Proof. According to Lemma 1, the quadratic H_∞ performance (15) can be obtained if and only if the conditions in Eq. (25) are satisfied. Considering the system matrices involve the time-varying matrix, thus Eq. (16) cannot be applied to design the controller. To eliminate it, the condition (16) can be rewritten by utilizing the Lemma 2, and then the condition (16) becomes the condition (25).

$$\Gamma + \bar{\Upsilon}\widehat{N}(t)\bar{\vartheta} + \bar{\vartheta}^T\widehat{N}(t)\bar{\Upsilon}^T < 0$$

where

$$\Gamma = \begin{bmatrix} \Xi & B_1(\rho) & C^T \\ * & -\eta^2 I & 0 \\ * & * & I \end{bmatrix}$$

$$\bar{\Upsilon}_1 = \begin{bmatrix} L_1(\rho) & L_3(\rho) \\ 0 & 0 \end{bmatrix}, \quad \widehat{N}_1(t) = \begin{bmatrix} \overline{N}(t) & 0 \\ 0 & \overline{N}(t) \end{bmatrix}, \quad \bar{\vartheta}_1 = \begin{bmatrix} H_1(\rho)R & 0 \\ 0 & H_3(\rho) \end{bmatrix}$$

$$\bar{\Upsilon}_2 = \begin{bmatrix} L_2(\rho) \\ 0 \end{bmatrix}, \quad \widehat{N}_2(t) = \overline{N}(t), \quad \bar{\vartheta}_2 = [H_2(\rho)R \quad 0 \quad 0]$$

Similarly, by using Lemma 2, the condition (23) becomes the condition (26), thus the proof is completed.

For the vehicle system, assuming that the bounds of the time-varying parameters ρ can presented by

$$\rho_\lambda = [\underline{\rho}_\lambda \bar{\rho}_\lambda], \quad \lambda = 1,2 \tag{27}$$

where $\bar{\rho}_\lambda$ and $\bar{\rho}_\lambda$ are the upper and lower bounds, since the state-space matrices of the LPV-based closed-loop system are linearly dependent on scheduled parameters ρ, thus $A_{\chi c}(\rho)$can be rewritten as

$$A_{\chi c}(\rho) = \sum_{i=1}^{4} \alpha_i(\rho) A_{\chi ci}(\omega_i) \tag{28}$$

where ω_i are the vertices of the polytope, and $\alpha_i(\rho)$ has the following form:

$$\alpha_i(\rho) = \frac{\prod_{\lambda=1}^{2} |\rho_\lambda - \theta(\omega_i)_\lambda|}{\prod_{\lambda=1}^{2} |\bar{\rho}_\lambda - \underline{\rho}_\lambda|} \tag{29}$$

where

$$\theta(\omega_i)_\lambda = \begin{cases} \bar{\rho}_\lambda, & \text{if } (\omega_i)_\lambda = \underline{\rho}_\lambda \\ \underline{\rho}_\lambda, & \text{otherwise} \end{cases}$$

and $\alpha_i(\rho)$ satisfy

$$\sum_{i=1}^{4} \alpha_i(\rho) = 1$$

Theorem 2. For the closed-loop system in (14), the gain-scheduling state-feedback controller exists such that the closed-loop system is quadratic D-stability in the disk centered at $(-q, 0)$ with a radius r and possesses quadratic H_∞ performance η form w to z for all variable values of the parameter vector ρ, if and only if there exist $\varepsilon_i(\rho)$, R_i and a symmetric positive definite matrix Q such as the following matrix inequalities are feasible:

$$\begin{cases} \Theta_{ij} + \Theta_{ji} < 0 \\ \Omega_{ij} + \Omega_{ji} < 0 \end{cases} \tag{30}$$

where

$$\Theta_{ij} = \begin{bmatrix} \Xi_i & B_{1,i}(\rho) & C_i^T & \varepsilon_{1,i}(\rho)L_{1,j}(\rho) & \varepsilon_{2,i}(\rho)L_{3,j}(\rho) & (H_{1,i}(\rho)R_i)^T & 0 & \varepsilon_{3,i}(\rho)L_{2,j}(\rho) & (H_{2,i}(\rho)R_i)^T \\ * & -\eta^2 I & 0 & 0 & 0 & 0 & (H_{3,i}(\rho))^T & 0 & 0 \\ * & * & -I & 0 & 0 & 0 & 0 & 0 & 0 \\ * & * & * & -\varepsilon_{1,i}(\rho)I & 0 & 0 & 0 & 0 & 0 \\ * & * & * & * & -\varepsilon_{2,i}(\rho)I & 0 & 0 & 0 & 0 \\ * & * & * & * & * & -\varepsilon_{1,i}(\rho)I & 0 & 0 & 0 \\ * & * & * & * & * & * & -\varepsilon_{2,i}(\rho)I & 0 & 0 \\ * & * & * & * & * & * & * & -\varepsilon_{3,i}(\rho)I & 0 \\ * & * & * & * & * & * & * & * & -\varepsilon_{3,i}(\rho)I \end{bmatrix}$$

$$\Omega_{ij} = \begin{bmatrix} -rQ & qQ + A_{\Xi i}(\rho)Q & \varepsilon_{5,i}(\rho)L_{1,j}(\rho) & 0 & \varepsilon_{6,i}(\rho)L_{2,j}(\rho) & 0 \\ * & -rQ & 0 & (H_{1,i}(\rho)Q)^T & 0 & (H_{2,i}(\rho)Q)^T \\ * & * & -\varepsilon_{4,i}(\rho)I & 0 & 0 & 0 \\ * & * & * & -\varepsilon_{4,i}(\rho)I & 0 & 0 \\ * & * & * & * & -\varepsilon_{5,i}(\rho)I & 0 \\ * & * & * & * & * & -\varepsilon_{5,i}(\rho)I \end{bmatrix}$$

Thus, designing the controller is completed, and the final gain can be obtained:

$$K(\rho) = \sum_{i=1}^{4} \alpha_i(\rho) R_i Q^{-1} \tag{31}$$

4. Simulation and analysis

CarSim® is a widely used dynamic software that can simulate and analyze the dynamic handling behavior of different vehicles under diversiform driving conditions. It incorporates a 27-degree-of-freedom full-vehicle model, which is equipped with nonlinear tire models and virtual sensors as a standard feature. It is worth noting that, two different vehicle models are presented for different purposes in this paper. In Section 2, the main purpose of establishing the uncertain vehicle dynamics model that derived from the single track model is to design robust gain-scheduled controller, while the high-fidelity, full-vehicle vehicle model obtained from CarSim® is used for simulation purposes. According to the parameters of the experimental electric vehicles in our laboratory, the simulation high-fidelity, full-vehicle vehicle model was obtained using CarSim®, and then utilizing Carsim® and co-simulation between Carsim® and Matlab/Simulink, the numerical simulation that includes single lane change, double lane change and sinusoidal steering maneuvers is implemented to verify and evaluate the performance of the designed controller.

4.1. Single lane change

Single lane change is implemented to evaluate the tracking performance and robustness against variation of tire cornering stiffness for the designed controller. In the simulation, the friction coefficient of the high-μ surface is set to be 0.9, and uncertainties in the stiffness of the front and rear tires are set to be ±25%. The simulation results including the steering wheel angle, longitudinal velocity, yaw rate and vehicle sideslip angle at the CG, and yaw moment are shown in Figs. 5–9. Compared with other research focused on the fixed longitudinal velocity, here the longitudinal velocity is time-varying. As shown in Fig. 6, the longitudinal velocity increases from 30 km/s to 37 km/s. It can be observed that the

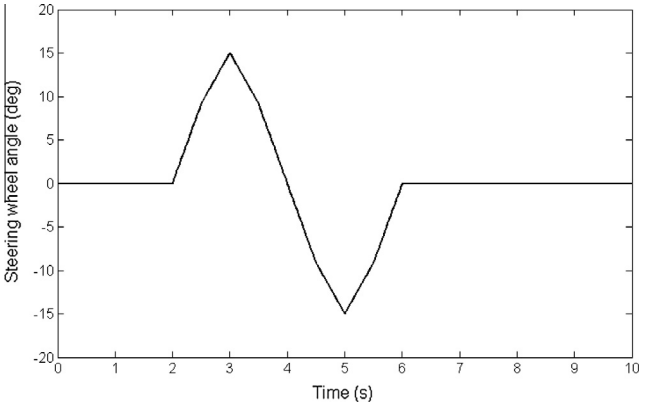

Fig. 5. Steering wheel angle for single lane change.

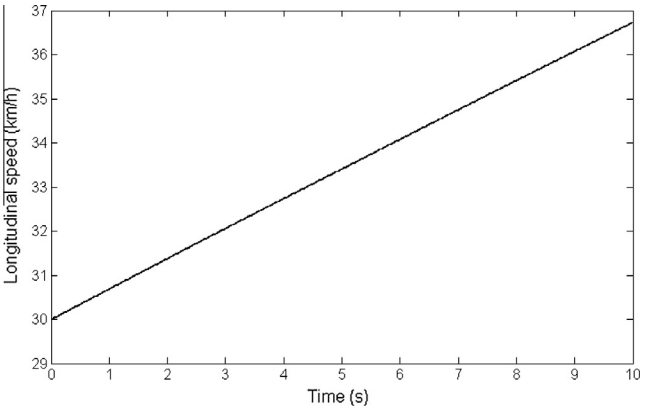

Fig. 6. Longitudinal velocity for single lane change.

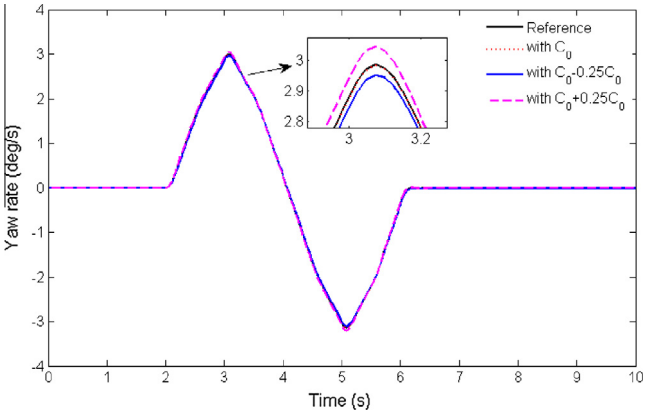

Fig. 7. Yaw rate for single lane change.

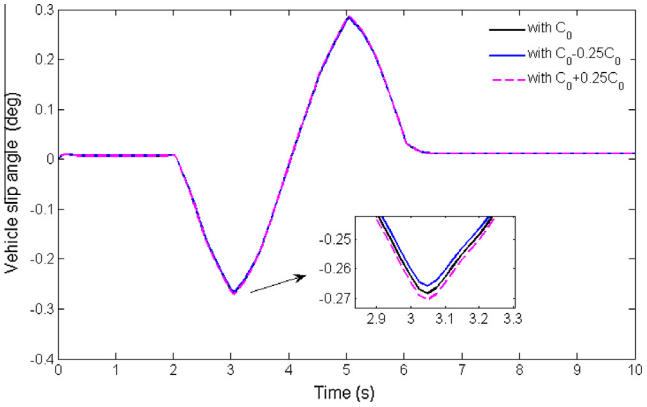

Fig. 8. Vehicle slip angle for single lane change.

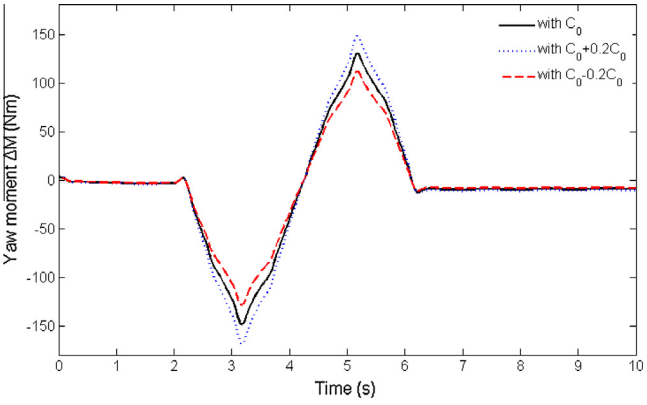

Fig. 9. Yaw moment for single lane change.

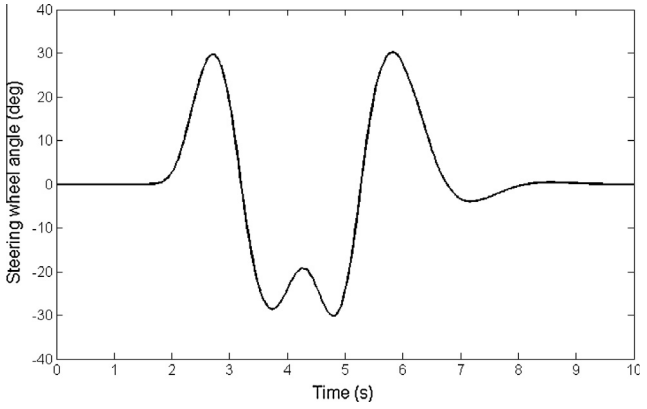

Fig. 10. Steering wheel angle for double lane change.

controlled yaw rate and vehicle sideslip angle at the CG are close to the desired references from Figs. 7 and 8, which means that the designed controller shows good tracking performance. Fig. 9 presents the external yaw moment controlled by the controller in single lane change simulation. As can be seen from Fig. 9, as long as the steering occurs, the controlled yaw moment quickly changes along with it, this phenomenon indicates that the controller has a satisfied transient response.

In addition, when the stiffness of the front and rear tires is heavily changed, only some small differences between the controlled states and the references can be observed from figures of partial enlargement, it can be clearly explained due to the strong robustness of the designed controller.

4.2. Double lane change

The main objective of double lane change simulation is to verify the effect of the designed controller for vehicle lateral stability control under extreme steering maneuvers, i.e. heavy steering under the low-μ surface. In this simulation, the friction coefficient of the low-μ surface is set to be 0.6, and uncertainties in the vehicle mass are set to be ±25%. The variable range of the longitudinal velocity shown in Fig. 11 changes from 65 km/h to 75 km/h. As

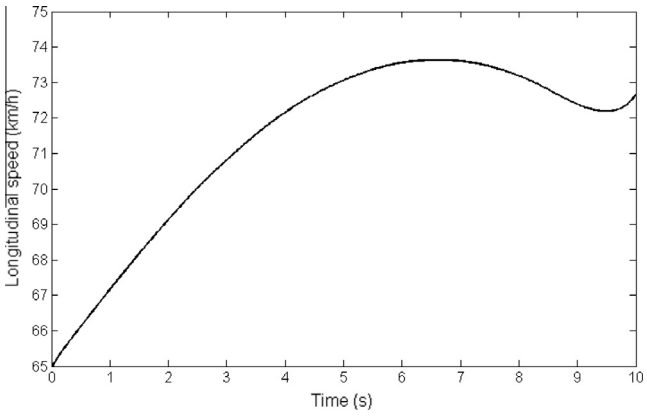

Fig. 11. Longitudinal velocity for double lane change.

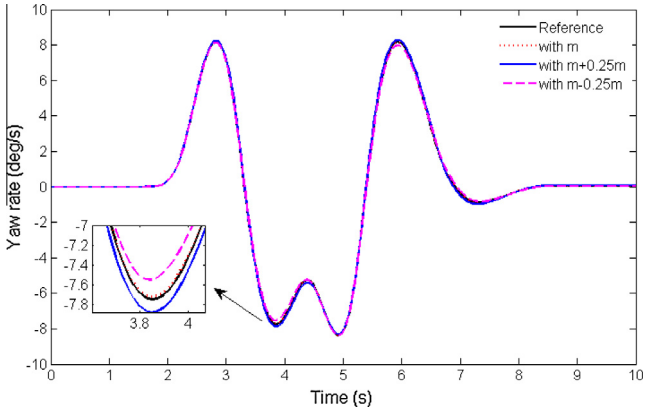

Fig. 12. Yaw rate for double lane change.

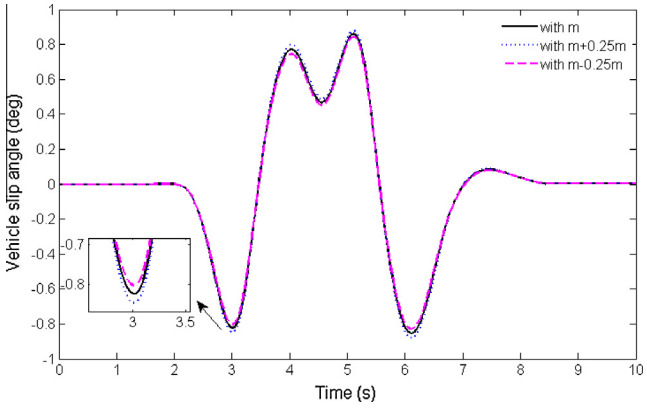

Fig. 13. Vehicle slip angle for double lane change.

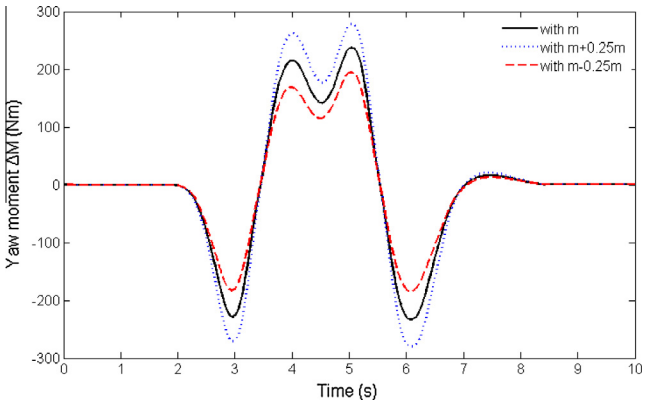

Fig. 14. Yaw moment for double lane change.

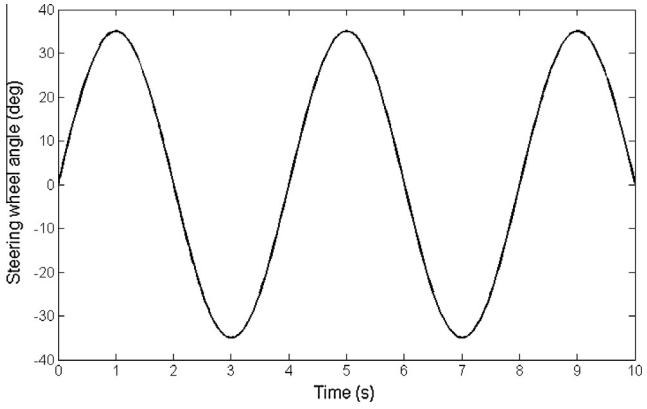

Fig. 15. Steering wheel angle for sinusoidal steering.

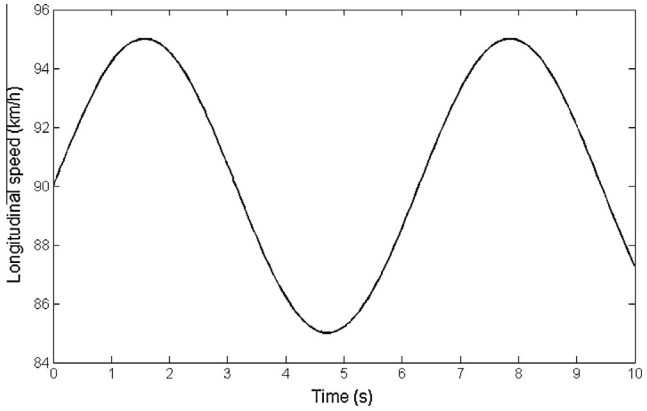

Fig. 16. Longitudinal velocity for sinusoidal steering.

can be seen in Fig. 10 and Figs. 12 and 13, when heavy steering with 30 degree occurs, the controlled yaw rate and vehicle sideslip angle at the CG still keep the good tracking performance even for vehicle mass with large variation. It also shows that the designed controller has strong robustness with respect to the vehicle mass variation. Fig. 14 shows the external yaw moment regulated by the designed controller, which changes as steering takes place, that is because that controller tries to compensate for tracking error.

4.3. Sinusoidal steering

The sinusoidal steering is carried out in the third maneuver. As shown in Fig. 15, the sinusoidal steering maneuver is more severe than the above two turning maneuver because the turning actions are more frequent and quicker, the turning maneuver is applied to further evaluate vehicle lateral stability and handling performance of the proposed *D*-stability-based robust gain-scheduled controller (DRGC). In this sinusoidal steering maneuver, the friction coefficient of the high-μ surface is set to be 0.9, and here the tire cornering stiffness shown in Fig. 17 is time-varying. The simulation results, including the longitudinal velocity, yaw rate and vehicle sideslip angle, are shown in Figs. 15 and 16 and Figs. 18 and 19.

To illustrate the benefit with *D*-stability, the proposed *D*-stability-based robust gain-scheduled controller and robust

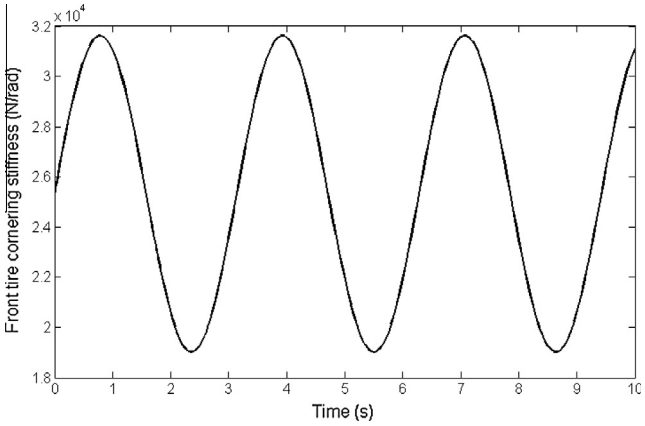

Fig. 17. Time-Varying front tire cornering stiffness for sinuso.

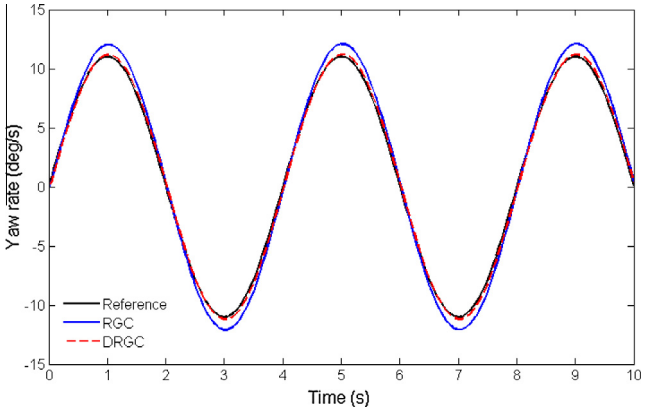

Fig. 18. Yaw rate for sinusoidal steering.

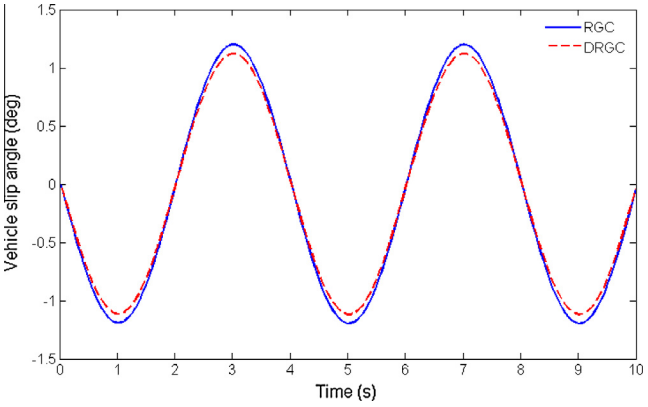

Fig. 19. Vehicle slip angle for sinusoidal steering.

gain-scheduled controller without *D*-stability (RGC) are compared in Figs. 18 and 19. As can be seen from Figs. 18 and 19, the proposed DRGC possesses better tracking performance for vehicle lateral dynamics system, whereas the RGC generates large error in the transient process. For instance, during the time interval (e.g., 2.5–3.5 s and 4.5–5.5 s), large error can be observed. This is owing to the fact that the *D*-stability was applied to improve the transient response of the closed-loop system. The sinusoidal steering maneuver also exhibits that the proposed controller can provide improved vehicle lateral stability even when the vehicle longitudinal velocity and tire cornering stiffness are time-varying.

In addition, comparing Figs. 8, 13 and 19, even though the controlled vehicle sideslip angle in double lane change and sinusoidal steering simulations shows larger values than that in single lane change simulation, the controlled vehicle sideslip angle tends to small (less than ±1.5 degree). It is necessary to mention that the vehicle sideslip angle is a critical index for evaluating the vehicle lateral stability, safety and handling performance. Generally, if the vehicle sideslip angle is too large, typically more than ±2 degree, the vehicle lateral stability may be lost. Thus, the controlled vehicle using the designed controller is stable, such a small vehicle sideslip angle indicates that vehicle lateral stability, safety and handling performance can be improved.

5. Conclusion

A robust gain-scheduled H_∞ controller for lateral stability control of FWID-EVs is proposed by using LPV technique. Uncertainties in vehicle dynamics model are analyzed, and the time-varying longitudinal speed in lateral stability control is also investigated. Simulation including single lane change, double lane change and sinusoidal steering maneuvers is implemented to verify the effectiveness of the proposed controller by using Matlab/Simulink-Carsim®. The simulation show that the designed controller possesses effectual tracking performance and strong robustness against uncertainties, which indicates that the designed controller can provide improved vehicle lateral stability, safety and handling performance. Although the simulation results has a certain guiding significance for real applications, perhaps the implementing effort of the proposed controller is very crucial for the real vehicle applications. Hence, the additional attention on effect of the implementing effort based on a simplified controller should be paid to further enhance vehicle performance in future works.

Acknowledgments

This work was supported by the National Natural Science Foundation of China (No. 51105074), the Foundation of State Key Laboratory of Automotive Safety and Energy, Tsinghua University (No. KF14192) and the Fundamental Research Funds for the Central Universities and Jiangsu Province postgraduate scientific research and innovation plan projects (No. KYLX_0103), and the Scientific Research Foundation of Graduate School of Southeast University and Southeast University Excellent Doctor degree Thesis Training Fund (No. YBJJ1429).

References

[1] Hori Y. Future vehicle driven by electricity and control-research on four-wheel-motored 'UOT Electric March II'. IEEE Trans Ind Electron Oct. 2004;51(5):954–62.
[2] Nam K, Fujimoto H, Hori Y. Advanced motion control of electric vehicles based on robust lateral tire force control via active front steering. IEEE/ASME Trans Mechatronic 2014;19(1):289–99.
[3] Wang J, Longoria RG. Coordinated and reconfigurable vehicle dynamics control. IEEE Trans Control Syst Technol May 2009;17(3):723–32.
[4] Shuai Z, Zhang H, Wang J, Li J, Ouyang M. Combined AFS and DYC control of four-wheel-independent-drive electric vehicles over CAN network with time-varying delays. IEEE Trans Veh Technol 2014;63(2):591–602.
[5] Yamakawa J, Ko jimaa A, Watanabe K. A method of torque control for independent wheel drive vehicles on rough terrain. J Terramech 2007;44(5):371–81.
[6] Yin G, Jin X, Qing Z, et al. Lateral stability region conservativeness estimation and torque distribution for FWIA electric vehicle steering. Sci China Technol Sci 2014;57(12):1–8.
[7] Cong G, Mostefai L, Denai M, Hori Y. Direct yaw-moment control of an in-wheel-motored electric vehicle based on body slip angle fuzzy observer. IEEE Trans Ind Electron May 2009;56(5):1411–9.
[8] Zhang H, Zhang X, Wang J. Robust gain-scheduling energy-to-peak control of vehicle lateral dynamics stabilisation. Veh Syst Dyn 2014;52(3):309–40.

[9] Piyabongkarn D, Rajamani R, Grogg J, Lew J. Development and experimental evaluation of a slip angle estimator for vehicle stability control. IEEE Trans Control Syst Technol Jan. 2009;17(1):78–88.
[10] Du H, Zhang N, Dong G. Stabilizing vehicle lateral dynamics with considerations of parameter uncertainties and control saturation through robust yaw control. IEEE Trans Veh Technol Jun. 2010;59(5):2593–7.
[11] Huang X, Wang J. Lightweight vehicle control-oriented modeling and payload parameter sensitivity analysis. IEEE Trans Veh Technol 2011;60(5):1999–2011.
[12] You S, Chai Y. Multi-objective control synthesis: an application to 4WS passenger vehicles. Mechatronics 1999;9(4):363–90.
[13] Yin G, Chen N, Li P. Improving handling stability performance of fourwheel steering vehicle via μ-synthesis robust control. IEEE Trans Veh Technol Sep. 2007;56(5):2432–9.
[14] Du H, Zhang N. Designing H_∞/GH_2 static-output feedback controller for vehicle suspensions using linear matrix inequalities and genetic algorithms. Veh Syst Dyn 2008;46(5):385–412.
[15] Zhou H, Liu Z. Vehicle yaw stability-control system design based on sliding mode and back stepping control approach. IEEE Trans Veh Technol Sep. 2010;59(7):3674–8.
[16] Wang J, Wang Q, Jin L, et al. Independent wheel torque control of 4WD electric vehicle for differential drive assisted steering. Mechatronics 2011;21(1):63–76.
[17] Ackermann J. Robust decoupling, ideal steering dynamics and yaw stabilization of 4WS cars. Automatica 1994;30(11):1761–8.
[18] He Z, Ji X. Nonlinear robust control of integrated vehicle dynamics. Veh Syst Dyn 2012;50(2):247–80.
[19] Zhang H, Shi Y, Wang J. On energy-to-peak filtering for nonuniformly sampled nonlinear systems: a Markovian jump system approach. IEEE Trans Fuzzy Syst 2014;22(1):212–22.
[20] Karimi H, Zapateiro M, Luo N. A linear matrix inequality approach to robust fault detection filter design of linear systems with mixed time-varying delays and nonlinear perturbations. J Franklin I 2010;347(6):957–73.
[21] Apkarian P, Gahinet P, Becker G. Self-scheduled H_∞ control of linear parameter-varying systems: a design example. Automatica 1995;31(9):1251–61.
[22] Lee C, Shin M, Chung M. A design of gain-scheduled control for a linear parameter varying system: an application to flight control. Control Eng Pract 2001;1:11–21.
[23] Apkarian P, Gahinet P. A convex characterization of gain-scheduled H∞ controllers. IEEE Trans Automatic Control 1995;40(5):853–64.
[24] Wang R, Wang J. Fault-tolerant control with active fault diagnosis for four-wheel independently-driven electric ground vehicles. IEEE Trans Veh Technol Nov. 2011;60(9):4276–87.
[25] Baslamisli SC, Kose IE, Anlas G. Gain-scheduled integrated active steering and differential control for vehicle handling improvement. Veh Syst Dyn Jan. 2009;47(1):99–119.
[26] Corno M, Savaresi S, Balas G. On linear-parameter-varying (LPV) slip-controller design for two-wheeled vehicles. Int J Robust Nonlinear Control 2009;19(12):1313–36.
[27] Poussot-Vassal C, Sename O, Dugard L, et al. Vehicle dynamic stability improvements through gain-scheduled steering and braking control. Veh Syst Dyn 2011;49(10):1597–621.
[28] Palladino L, Duc G, Poth R. LPV control for mu-split braking assistance of a road vehicle. In: Proc. IEE decision and control conf.; 2005. p. 2664–2669.
[29] Mammar S. Two-degree-of-freedom H_∞ optimization and scheduling for robust vehicle lateral control. Veh Syst Dyn 2000;34(6):401–22.
[30] Wang Y, Nguyen BM, Fujimoto H, Hori Y. Multirate estimation and control of body slip angle for electric vehicles based on onboard vision system. IEEE Trans Ind Electron 2014;61(2):1133–43.
[31] Jin X, Yin G. Estimation of lateral tire-road forces and sideslip angle for electric Vehicles using interacting multiple model filter approach. Int J Franklin Inst http://dx.doi.org/10.1016/j.jfra nklin.2014.05.008.
[32] Karimi H. Observer-based mixed H_2/H_∞ control design for linear systems with time-varying delays: an LMI approach. Int J Control Autom Syst 2008;6(1):1–14.
[33] Zhang H, Shi Y, Saadat Mehr A. Robust static output feedback control and remote PID design for networked motor systems. IEEE Trans Ind Electron 2011;58(12):5396–405.